

The Added Value of Longitudinal Imaging for Preclinical In vivo Efficacy Testing of Therapeutic Compounds against Cerebral Cryptococcosis

Liesbeth Vanherp, Jennifer Poelmans, Amy Hillen, Guilhem Janbon, Matthias Brock, Katrien Lagrou, Greetje Vande Velde, Uwe Himmelreich

▶ **To cite this version:**

Liesbeth Vanherp, Jennifer Poelmans, Amy Hillen, Guilhem Janbon, Matthias Brock, et al.. The Added Value of Longitudinal Imaging for Preclinical In vivo Efficacy Testing of Therapeutic Compounds against Cerebral Cryptococcosis. Antimicrobial Agents and Chemotherapy, 2020, 64 (7), pp.e00070-20. 10.1128/AAC.00070-20 . pasteur-02652024

HAL Id: pasteur-02652024
https://pasteur.hal.science/pasteur-02652024

Submitted on 29 May 2020

HAL is a multi-disciplinary open access archive for the deposit and dissemination of scientific research documents, whether they are published or not. The documents may come from teaching and research institutions in France or abroad, or from public or private research centers.

L'archive ouverte pluridisciplinaire **HAL**, est destinée au dépôt et à la diffusion de documents scientifiques de niveau recherche, publiés ou non, émanant des établissements d'enseignement et de recherche français ou étrangers, des laboratoires publics ou privés.

Title page

Title

The Added Value of Longitudinal Imaging for Preclinical *In vivo* Efficacy Testing of Therapeutic Compounds against Cerebral Cryptococcosis

Running title

In vivo imaging of anticryptococcal treatment in mice

Authors

Liesbeth Vanherp[a,b], Jennifer Poelmans[a,b,°], Amy Hillen[a,b,◊], Guilhem Janbon[c], Matthias Brock[d], Katrien Lagrou[e,f], Greetje Vande Velde[a,b,#,*], Uwe Himmelreich[a,b,*]

Address correspondence to Greetje Vande Velde, greetje.vandevelde@kuleuven.be

* G.V.V. and U.H. contributed equally to this work

Affiliations

[a] Biomedical MRI, Department of Imaging and Pathology, KU Leuven, Leuven, Belgium

[b] Molecular Small Animal Imaging Center (MoSAIC), KU Leuven, Leuven, Belgium

[c] RNA Biology of Fungal Pathogens, Department of Mycology, Pasteur Institute, Paris, France

[d] Fungal Biology Group, School of Life Sciences, University of Nottingham, Nottingham, United Kingdom

[e] Laboratory of Clinical Bacteriology and Mycology, Department of Microbiology, Immunology and Transplantation, KU Leuven, Leuven, Belgium.

[f] National Reference Centre for Mycosis, Department of Laboratory Medicine, University Hospitals Leuven, Leuven, Belgium

° Present address: The Janssen Pharmaceutical Companies of Johnson & Johnson, Beerse, Belgium

◊ Present address: Department of Cell and Molecular Biology (CMB), Karolinska Institutet, Stockholm, Sweden

Abstract

Brain infections with *Cryptococcus neoformans* are associated with significant morbidity and mortality. Cryptococcosis typically presents as meningoencephalitis or fungal mass lesions called cryptococcomas. Despite frequent *in vitro* discoveries of promising novel antifungals, the clinical need for drugs that can more efficiently treat these brain infections remains. A crucial step in drug development is the evaluation of *in vivo* drug efficacy in animal models. This mainly relies on survival studies or post-mortem analyses in large groups of animals, but these techniques only provide information on specific organs of interest at predefined time points. In this proof-of-concept study, we validated the use of non-invasive preclinical imaging to obtain longitudinal information on the therapeutic efficacy of amphotericin B or fluconazole monotherapy in meningoencephalitis and cryptococcoma mouse models. Bioluminescence imaging (BLI) enabled the rapid *in vitro* and *in vivo* evaluation of drug efficacy while complementary high-resolution anatomical information obtained by magnetic resonance imaging (MRI) of the brain allowed a precise assessment of the extent of infection and lesion growth rates. We demonstrated a good correlation between both imaging readouts and the fungal burden in various organs. Moreover, we identified potential pitfalls associated with the interpretation of therapeutic efficacy based solely on post-mortem studies, demonstrating the added value of this non-invasive dual imaging approach compared to standard mortality curves or fungal load endpoints. This novel preclinical imaging platform provides insights in the dynamic aspects of the therapeutic response and facilitates a more efficient and accurate translation of promising antifungal compounds from bench to bedside.

Introduction

Fungal infections of the central nervous system (CNS) are generally associated with high mortality rates and poor prognosis (1). The group of patients at risk for contracting these opportunistic infections has grown due to the increased prevalence of disease-induced or treatment-related immunosuppression (2). Of the few fungal species able to infect the brain, *Cryptococcus neoformans* is worldwide one of the most common causative organisms (2). It infects mainly HIV-patients, but also persons with underlying medical conditions or receiving immunosuppressive treatment, and occasionally immunocompetent individuals (3). Cryptococcal infection of the CNS arises after dissemination or reactivation of fungal cells that were initially acquired through inhalation. Most frequently, the disease presents as a subacute meningoencephalitis, with small accumulations of yeasts in the brain parenchyma (4, 5). More rarely, it causes mass lesions in the brain parenchyma, called cryptococcomas (1). These occur more frequently in immunocompetent patients due to the local containment of infection by the host response (6, 7).

Despite some recent progress in the development of novel antifungals, current treatment for cerebral cryptococcosis still uses drugs that were developed several decades ago (8, 9). The standard induction regimen combines the fungicidal polyene amphotericin B (AMB) with 5-fluorocytosine (10, 11). However, these drugs are not widely available and require intravenous administration and careful monitoring for drug-related toxicity. For these reasons, they are sometimes replaced by the oral drug fluconazole (FLC) in resource-limited settings, but monotherapy with this fungistatic drug is less efficacious (12). Despite recent advances in optimizing accessible combination therapies (13), the clinical need for effective, low-cost and widely available anticryptococcal drugs with minimal toxicity remains high (14).

Although new candidate drugs are frequently reported following *in vitro* screenings, only a very limited amount of these eventually reaches the clinic. For CNS infections, the presence of the blood-brain barrier (BBB) poses an additional hurdle in drug development. Even of the currently available antifungal compounds, only a few can efficiently reach the brain tissue (15).

To ensure an optimal translation from bench to bedside, testing the *in vivo* efficacy of a drug in animal models remains a crucial step as it allows studying the therapeutic response in a complex yet controlled system (16). Mammalian models allow the evaluation of therapy in the presence of an immune system and blood-brain barrier that is comparable to humans, including their potential disease-related changes. In murine models, response to antifungal treatment is frequently evaluated using survival curves, post-mortem colony-forming unit (CFU) analysis of the fungal load or histopathologic examination of the isolated organs (16, 17). However, these techniques pose some challenges as they only provide single endpoint measurements of the disease status and limited information about spatial distribution of disease. When a temporal profile of drug efficacy is required, these studies rely on large groups of animals in order to isolate specific organs at predefined time points.

More recently, non-invasive imaging techniques have been developed that allow longitudinal evaluation of the fungal infection status or treatment response in individual animals. Bioluminescence imaging (BLI) measures the light emitted from the oxidation of a substrate by an enzyme such as *Gaussia* or firefly luciferase. Numerous studies have shown and extensively validated that the measured signal is proportional to the number of cells expressing the luciferase and their viability (18–23), as intracellular ATP of living cells is essentially required for the light-emitting reaction of the firefly luciferase (24). By genetically engineering fungi to express this

luciferase reporter gene, the *in vitro* activity of antifungal compounds (19, 23, 25) and the temporal and spatial distribution of the infectious burden in living animals can be monitored (23, 26–28). In this respect, treatment studies using animal models of aspergillosis and candidiasis have shown a good correlation between traditional CFU analysis of the fungal load and treatment effects observed in various organs by using BLI (19, 26, 27, 29). Previously, we have developed and validated the use of a novel bioluminescent *Cryptococcus neoformans* strain for tracking pathogen dissemination from the lung to the brain (28). Hereby, we demonstrated a clear correlation between the number of CFUs and the emitted light, both *in vitro* and *in vivo*. Furthermore, magnetic resonance imaging (MRI) of the brain allowed a detailed analysis of the spatial distribution of infectious foci. However, to date, preclinical imaging techniques have not been used to monitor antifungal treatment efficacy against fungal infections of the CNS, such as cryptococcosis.

In this study, we assessed the use of BLI for screening the *in vitro* efficacy of antifungal compounds against *C. neoformans.* Secondly, we evaluated the combination of whole-body BLI and brain MRI to non-invasively monitor *in vivo* antifungal treatment efficacy with temporal and spatial resolution and validated this against standard CFU endpoint measurements. To this end, we tested liposomal AMB (L-AMB) or FLC monotherapy in murine models reflecting two distinct presentations of cerebral cryptococcosis: (i) a standard model of cryptococcal meningoencephalitis following disseminated disease and (ii) a model of a local cryptococcoma. In both cases, the treatment was delayed until BLI revealed that established disease was present. This late initiation of therapy was applied as it is similar to the clinical setting in which patients often present with advanced infection before being diagnosed. By obtaining longitudinal information on the dynamic

process of treatment response in individual animals, we aimed to demonstrate the potential, validity and added value of using non-invasive imaging in preclinical drug testing for fungal brain infections.

Results

In vitro bioluminescence assays enable rapid real-time assessment of fungicidal and fungistatic antifungal drug activity

To validate the potential of BLI to follow-up antifungal effects on cryptococcal cells, the bioluminescence emitted by *C. neoformans* reporter cells was measured *in vitro* at several time points after addition of amphotericin B deoxycholate (AMB-d) and fluconazole (FLC) (Fig. 1). The BLI signal intensity of the untreated cells highly increased in the beginning (0-6h), followed by a stable signal measured at 8 and 24h and a subsequent decline in aging cultures. After addition of AMB-d (0.1 mg/ml), bioluminescence decreased to background levels within two hours, indicating a rapid fungicidal effect of this drug at the tested concentration. Upon addition of the fungistatic drug FLC (0.5 mg/ml), the emitted bioluminescence initially continuously increased, but stagnated after 4 hours, followed by a decrease after 24 hours.

AMB induces a transient increase in bioluminescence that is potentially mediated by enhanced permeability for D-luciferin

After confirming the ability to detect antifungal effects using bioluminescence, we characterized the temporal profile of the bioluminescence signal in response to a wide concentration range of antifungals using a similar *in vitro* set-up. At 8 and 26 hours after exposure, a dose-dependent decrease in bioluminescence was observed for all tested concentrations of AMB-d and L-AMB, corresponding to its fungicidal effect (Fig. 2A-B, Fig. S1). When using the fungistatic agent FLC, the bioluminescence increased more slowly in cells exposed to higher concentrations (Fig. 2C, Fig. S1). At 8 hours, we observed a dose-dependent reduction of bioluminescence compared to the control.

Bioluminescence transiently increased immediately after the addition of AMB-d or L-AMB, while a similar effect was not observed for FLC (Fig. 2, S1). Higher doses of AMB induced a larger and more rapid increase, which was smaller and more delayed for L-AMB compared to AMB-d.

We investigated potential explanations for this increased bioluminescence in parallel experiments, using a *C. neoformans* strain with a fluorescent E2-Crimson reporter gene under control of the same promoter. Addition of the antifungals induced only a slight decrease in fluorescence, whereby the dose-dependent antifungal effect was most notable for FLC (Fig. S2). We did not observe increased fluorescence upon addition of the antifungals, indicating that a change in the expression levels of the reporter gene was not the cause of the increased bioluminescence. Furthermore, we found that none of the tested antifungals was auto-luminescent or auto-fluorescent in water or Sabouraud medium (Fig. S3), nor caused luminescence in wild-type *C. neoformans* cells (Fig. S4).

Since AMB affects the integrity of the cell membrane and induces transmembrane channels (30, 31), we hypothesized that this transient bioluminescence increase might be caused by enhanced permeability of the fungal cells for the substrate D-luciferin (32). Exposure to natamycin, a polyene antifungal that does not permeabilize the plasma membrane (33), led to a dose-dependent decrease in bioluminescence corresponding to its antifungal effect (Fig. 2D, Fig. S1). Only at the highest concentration tested (100 µg/ml), we observed a transient increase prior to this decrease. Exposure to SDS, a surfactant leading to destruction of cell integrity and cell death, induced a rapid and dose-dependent reduction of bioluminescence (Fig. 2E, Fig. S1).

Whole-body BLI allows simultaneous evaluation of drug efficacy at multiple body sites in a model of disseminated cryptococcosis

We subsequently validated the use of BLI and MRI for *in vivo* evaluation of antifungal treatment efficacy by using different treatment regimens in a standard model of advanced cryptococcal meningoencephalitis following disseminated disease (Fig. 3A). After i.v. injection of cryptococci, control animals developed a progressive infection in the brain and the abdomen, including the spleen and kidney region, as previously described (28) (Fig. 4). The baseline infection status was assessed on day 3 and this identified an unsuccessful induction of infection in one animal of the FLC-treated group. Treatment with L-AMB significantly reduced the infection in the abdomen, while the bioluminescence from the brain was comparable to the control group. We observed a higher brain and abdomen bioluminescence in L-AMB treated animals than control animals specifically on day 4 p.i., when imaging was performed less than three hours after injection of antifungals. Animals treated with FLC showed a significant delay in the development of high brain signal intensity until day 6 p.i., after which the signal increased. The bioluminescence from the abdominal region was reduced compared to the control group, except for one animal that presented with a persistent hotspot in all images.

MR imaging of the brain showed that disease progression is associated with an increase in the total lesion volume, number of brain lesions and average volume per lesion (Fig. 5). L-AMB treatment induced a small reduction in the total lesion volume, but not in the number of brain lesions or their average volume. The MRI on day 4 p.i. did not show a difference between the L-AMB treated and control animals that could explain the higher BLI signal intensity observed for the former group. Animals treated with FLC presented with a significantly lower total lesion volume and a smaller

average lesion volume compared to untreated or L-AMB treated animals. This was confirmed in lesion volume distributions obtained on day 6 (Fig. S5).

In agreement with the imaging results, CFU analysis showed that L-AMB led to a large reduction of the fungal load in the spleen and kidneys, while having a limited effect in the brain (Fig. 6). In comparison, FLC led to a larger reduction of the brain fungal load but had a more limited effect in the spleen and kidney. Quantitative cross-correlation of imaging results and CFU counts indicated that BLI results of the abdomen correlated well with the fungal load in the spleen and kidneys (Fig. S6). In the brain, the lesion volume quantified from the 3D MRI was highly correlated with the fungal load. On day 7 p.i., we could not detect a significant correlation between the BLI results and the brain fungal burden, mainly due to the limited differences in the BLI signal. Nevertheless, we found that the BLI results on day 6 were predictive for the fungal burden on day 7, as evidenced by their good correlation.

BLI and MRI provide highly complementary information about the individual response to systemic therapy in a cryptococcoma model

In a second proof-of-concept study, we tested the combination of *in vivo* BLI and MRI for monitoring treatment efficacy in a mouse model of a local cryptococcoma (Fig. 3 B). At baseline (day 3), established cryptococcomas were present in the mouse brains, with detectable bioluminescence and hyperintense focal lesions on the MR images (Fig. 7). The brain BLI signal intensity of untreated animals progressively increased (Fig. 7 A, C) and was paralleled by an increase in the lesion volume on MRI (Fig. 7 B, D). A single i.v. high dose of L-AMB showed no obvious treatment success. In contrast, animals treated with FLC generally presented with lower bioluminescence signal intensities and smaller brain lesions, indicating a response to antifungal therapy. Daily i.p. injections with L-AMB led to large inter-animal variability

in the response. The animal with the smallest lesion at baseline showed low bioluminescence and limited lesion growth on MRI. One animal showed a limited increase in bioluminescence, while the lesion volume increased substantially. The other two animals presented with a large increase in BLI signal, but this was not associated with larger brain lesions on MRI. However, MRI indicated that the infection was no longer confined to the induced lesion and had spread into the ventricle or towards the forebrain. The same was observed for one animal in the FLC-group. Histology confirmed that this presentation of the disease on MRI is typically associated with presence of cryptococci in the ventricles (Fig. S7).

After the last imaging session on day 9, CFU analysis showed an approximate tenfold reduction in the brain fungal load of most animals receiving daily L-AMB or FLC, although this difference was not significant (Fig. 8A). Invasion of the lesion into the ventricle was not associated with a higher fungal burden, except for one animal where infection had also spread to the forebrain. The *in vivo* BLI results correlated well with the fungal burden in the brain (Fig. 8B), and exclusion of the few animals with ventricular involvement further strengthened this correlation. Furthermore, we found good correspondence between fungal burden and lesion volume on MRI (Fig. 8C).

Intracerebral amphotericin B treatment shows limited efficacy in the cryptococcoma model

Due to the limited antifungal effect observed in the cryptococcoma model upon systemic treatment with L-AMB, we subsequently evaluated the efficacy of direct intracerebral injection delivering L-AMB in the cryptococcoma, as this would bypass the role of the blood-brain-barrier (BBB) in drug delivery (Fig. 3C). Similar to the control group, the brain BLI signal intensity increased for most animals in the L-AMB

253 group, except for animal 1 and 2 that showed a stagnated BLI signal on day 10 (Fig.
254 9A, C). In contrast, the lesion volume increased for all animals (Fig. 9B, D). On some
255 MR images, a small hyperintensity could be seen inside the lesion due to the
256 injection. Its limited size compared to the whole lesion size could indicate that only
257 part of the lesion was effectively targeted. CFU analysis showed a small but
258 significant reduction in the fungal load, with limited variability within the group (Fig.
259 S8). Although animal 1 and 2 showed a response on BLI, their fungal burden and
260 lesion volume was similar to the other animals. This indicates that intracerebral
261 injection of L-AMB in this cryptococcoma model is not superior to intraperitoneal
262 delivery of the drug.

Discussion

In this work, we have demonstrated that BLI enables qualitative and quantitative evaluation of the *in vitro* and *in vivo* therapeutic efficacy of antifungal compounds against *C. neoformans.* MRI provided a complementary readout on treatment effects by monitoring the spatial distribution and growth rate of lesions in the brain. Both BLI and MRI results were in good agreement with CFU analysis, allowing a non-invasive *in vivo* assessment of the fungal load. In contrast to single time point measurements such as CFU analysis or histology, this novel approach provides information about the temporal and spatial evolution of the infection and therapeutic response in living animals and allows studying multiple infections sites simultaneously. Moreover, longitudinal imaging is non-invasive and reduces the number of animals needed for the preclinical evaluation of antifungal therapy as individual animals can be monitored throughout the full disease and treatment process. Therefore, the implementation of preclinical imaging can raise the ethical acceptance of *in vivo* efficacy studies, which remain an essential step for the evaluation of novel therapeutic compounds.

BLI enabled rapid real-time screening of *in vitro* antifungal drug efficacy with distinction between fungistatic and fungicidal activity. The use of real-time imaging techniques for determination of drug sensitivity and time-kill curves has the advantage that plating of samples for CFU counting can be neglected and results are obtained immediately (34). This makes BLI an interesting alternative for rapid real-time *in vitro* assessment of antifungal activity, and multiplexing BLI with fluorescence or dye-based approaches can provide additional validation of the results (19, 34). As some drugs induced a temporal increase in bioluminescence, robust testing of the antifungal effect should be done a broader time window to avoid measuring only

these difficult to interpret transient effects. Alterations in membrane permeability causing an increased substrate influx are a possible contributor, and previous studies have used luciferase reporters to assess cell permeabilization in bacteria (32). Further study is warranted to investigate how this transient increase relates to the complex mode of action of antifungals, and whether similar effects are also present with other bioluminescent organisms.

Subsequently, we aimed to validate a combination of non-invasive optical and anatomical imaging for *in vivo* evaluation of antifungal treatment efficacy in two mouse models and compared these to standard endpoint measurements such as CFU counts to quantify fungal load. Both BLI and MRI readouts correlated well with the fungal burden in various organs, indicating that our dual imaging approach represents a valuable non-invasive alternative, or at least compatible addition, to the traditional post-mortem techniques. Even more so, our findings indicated that results from endpoint analyses can lead to misinterpretation of treatment effects and showed that these limitations can be overcome using non-invasive imaging. In the disseminated disease model, the therapeutic response was variable throughout the disease period, indicating that the selection of specific time points for fungal load analysis and correct identification of infected body sites (such as brain versus kidney infection) can have a large impact on conclusions about *in vivo* drug efficacy. Furthermore, our approach qualitatively and quantitatively assessed the infection status of individual animals prior to the start of treatment and identified animals in which induction of infection had failed, which might be wrongly interpreted as treatment success in single time point analyses. In addition, whole-body BLI allowed simultaneous assessment of the antifungal efficacy in various organs, including organs that were not in primary focus of this study. This contrasts techniques like

CFU counting or histology, where effects are only studied in predefined organs. Hence, the implementation of this dual imaging approach in preclinical drug efficacy testing for CNS infections allows a more efficient and more complete assessment of the therapeutic effect than the standard techniques.

Overall, our BLI readouts correlated well to the current gold standard of CFU analysis, but for correct interpretation of BLI results it remains important to realize that several confounding factors may limit a direct translation from BLI signal to viable fungal load. First, the localization of infection affects the amount of detectable light. The BLI signal was higher when infection had spread to the ventricles and CSF compared to deep-seated, localized cryptococcomas, although this was not associated with an increased fungal load. Secondly, the bioluminescence reaction using firefly luciferases requires the availability of D-luciferin and the cofactors O_2, ATP and Mg^{2+}. Especially in larger or necrotic lesions, the delivery of oxygen and the substrate D-luciferin might be limited, leading to a lower signal intensity (22). Changes in the BBB-integrity could also affect the permeability for D-luciferin (35). Finally, we showed that some drugs may cause a transient BLI increase potentially due to altered membrane permeability and luciferin uptake, which could result in reduced correlation of the BLI signal with CFU counts. Our study illustrated that performing *in vivo* experiments in this specific time window of transient effects may lead to a transiently increased bioluminescence that is not necessarily related to an increased fungal load.

The addition of MRI provided a valuable second readout on treatment efficacy by monitoring with high spatial detail how antifungal treatment affects the growth rate and spatial distribution of brain lesions and limits damage to the host brain. In the meningoencephalitis model, MRI allowed the detailed analysis of the number of brain

lesions and their respective size and showed an excellent correlation with the fungal load in the brain. Although MRI was able to demonstrate a slower growth rate of lesions upon treatment, successful antifungal therapy will most likely not result in rapid shrinkage of the lesion, as has also been shown in clinical MR studies (36). As the hyperintense contrast on MRI is not specifically generated by viable fungi, the result of antifungal treatment will likely show a delayed response on MRI, in contrast to BLI where a direct effect on fungal cell viability can be observed. But, in contrast to BLI, MRI does not require genetic modification of the fungal strain and is also implemented in a clinical setting.

The highly complementary information obtained by the combination of BLI and MRI can overcome the limitations of the individual imaging techniques. Our study showed that this is extremely valuable for correct interpretation of results. The acquired whole-body BLI images can be used to monitor and quantify the differential spatial and temporal distribution of infection and treatment effects in multiple organs simultaneously. BLI can guide additional anatomical imaging techniques towards organs of interest to obtain a detailed 3D localization of the infectious foci. MRI can provide an alternative readout on the infection status to validate the BLI results and identify potential reasons for specific observations with BLI. As an example, MRI showed the spatial distribution of infection towards the ventricles, or can detect bleeding or scar tissue which may attenuate the emitted light. In this way, BLI and MRI provide highly complementary information on different aspects of the therapeutic response: the direct effect on viable fungal load (BLI) or on lesion growth and damage to the host (MRI).

We have validated this novel imaging approach in two different animal models of cryptococcosis that represent two distinct clinical presentations of the disease.

Treatment was generally less effective in the cryptococcoma model than the meningoencephalitis model, most likely due to limited drug penetration in large lesions. This corresponds to clinical case reports, where cryptococcomas are typically difficult to treat and require prolonged antifungal treatment and sometimes surgical resection (10, 37, 38). Moreover, meningoencephalitis models have a demonstrated impairment of the BBB-integrity leading to more efficient penetration of AMB (39, 40), while this has not yet been investigated in cryptococcoma models. Preclinical studies using this model could help to optimize clinical treatment strategies for cryptococcomas.

Our current study validated the use of *in vivo* imaging techniques for non-invasive testing of treatment efficacy in various organs. It was not a direct aim of this proof-of-concept study to identify the most optimal treatment regimens for cryptococcosis. Accordingly, our study was sufficiently powered to demonstrate visually observable treatment effects with statistical validity, but a larger number of animals would likely be required for detecting potential more subtle effects. Our results indicated that the applied monotherapy regimens were insufficient to effectively clear the infection from all body sites. One reason for this limited efficacy of treatment can be attributed to the late start of therapy, which was initiated when disease had already been manifested. Such a limited efficacy of antifungal treatment has also been reported in other models with delayed treatment (26, 41), and underlines the importance of early diagnosis and rapid initiation of therapy (42, 43). Nonetheless, our results showed that *in vivo* antifungal efficacy in various organs can largely be attributed to the known biodistribution of the tested compounds. In the disseminated disease model, the potent fungicidal drug L-AMB reduced the infection load in the kidney and eradicated all cryptococci from the spleen, which is consistent with its high tissue concentration

388 in this organ (44, 45). This was in contrast to the brain, where the best results were
389 obtained using FLC, a drug that effectively crosses the BBB. I.p. injection with L-AMB
390 only mildly reduced brain fungal load, consistent with its low availability in the brain
391 which may hamper efficient control of CNS infections (15, 45). A higher treatment
392 efficacy in the brain could potentially be achieved by i.v. injection of L-AMB through
393 increased systemic uptake, although daily i.v. injections in mice are technically more
394 challenging. An earlier initiation, prolonged treatment or combination therapy with
395 different antifungals would likely also enhance treatment efficacy, and many different
396 combinations and regimens have previously been evaluated in animal studies and
397 clinical trials. Our proof-of-concept study shows that preclinical imaging is sensitive
398 enough to detect even small treatment effects. As such, this work can form the basis
399 for additional follow-up studies that search the most effective treatment strategy by
400 use of preclinical imaging in appropriately powered animal studies.

401 In conclusion, we have shown that BLI and MRI allow non-invasive evaluation of the
402 *in vivo* efficacy of antifungal compounds combatting CNS cryptococcosis. Both *in*
403 *vitro* and *in vivo* BLI allowed for the rapid real-time assessment of the viable fungal
404 load and its response to therapy, while treatment effects in multiple organs could be
405 evaluated simultaneously. MRI allowed monitoring of the spatial distribution and
406 growth rate of the brain lesions following antifungal treatment. The combination of
407 both techniques provided highly complementary information and allowed longitudinal
408 monitoring of the treatment effects in individual animals. This approach proved to be
409 a powerful tool that can reveal important aspects of the dynamics of treatment
410 response, which could be missed by single time point measurements like CFU and/or
411 survival analyses and potentially lead to misinterpretation of therapeutic drug
412 efficacy. Therefore, non-invasive *in vivo* imaging techniques have the potential to

help improve the efficiency and accuracy of preclinical drug testing for CNS infections and accelerate the translation of promising drug candidates or treatment regimens to the clinic.

Material and methods

Fungal strains

The bioluminescent *C. neoformans* KN99α strain (28) expressing a red-shifted, codon-optimized firefly luciferase was used for both *in vitro* and *in vivo* experiments. Additional *in vitro* experiments were performed using a wild-type and red fluorescent *C. neoformans* KN99α strain, expressing the protein E2-Crimson (see supplementary methods for construction of this strain). A GFP-expressing *C. neoformans* H99 strain (46) was used for histology of the infected brains. All *Cryptococcus* strains were cultured on Sabouraud agar (Bio-Rad, Temse, Belgium) for 2-3 days at 37°C (*in vitro*) or 30°C (*in vivo* experiments) prior to transfer to liquid cultures.

In vitro experiments

Bioluminescence assay of antifungal effects

Liquid cultures were grown in DYP medium (1 % glucose, 0.5% yeast extract, 1% peptone) for 24 hours at 37°C while shaking (200 rpm). Amphotericin B deoxycholate (AMB-d, 0.1 mg/ml, Fungizone, Bristol-Myers Squibb, Utrecht, The Netherlands), fluconazole (FLC, 0.5 mg/ml, TCI Europe, Zwijndrecht, Belgium) or an equal volume of sterile water (control) was added to the culture. Both drugs were dissolved or dispersed in sterile water. Cultures (10 ml) were incubated at 37°C while shaking and samples were measured immediately after, 2, 4, 6, 8, 24, 48 and 72 hours after

addition of the antifungals. The results are expressed relative to the average signal obtained immediately after addition of the drug to normalize for differences in initial culture density.

Temporal profile of bioluminescence after antifungal therapy

Cultures were inoculated in liquid Sabouraud medium (Bio-Rad) and grown for 20 hours at 37°C while shaking. AMB-d, liposomal amphotericin B (L-AMB, AmbiSome, Gilead Sciences, Carrigtohill, Ireland), FLC, natamycin (JK Scientific GmbH, Pforzheim, Germany) or sodium dodecyl sulphate (SDS, Merck, Hohenbrunn, Germany) were dissolved or suspended in sterile water. Antifungal compounds were added to aliquots (4 ml) of the cultures at a final concentration of 0.01, 0.1, 1, 10 or 100 µg/ml, while SDS was used at 1, 0.1, 0.01, 0.001 and 0.0001 %. An equal volume of sterile water was added to the no drug control. Bioluminescence was measured at 5 minutes, 40 minutes, 1, 2, 4, 6, 8 and 26 hours after antifungal addition.

In vitro bioluminescence and fluorescence measurements

100 µl of the culture was transferred to a 96-well plate (Falcon Microtest 96, Becton Dickinson, Meylan Cedex, France) and 100 µl of D-luciferin (final concentration 0.15 µg/ml, in phosphate-buffered saline (PBS), Luciferin-EF, Promega, USA) was added. Bioluminescence was measured in triplicate or quadruplicate samples using a plate reader (Wallac Victor 1420, Perkin Elmer, Waltham, USA) with 10 seconds measurement time. For assessment of fluorescent E2-Crimson strains, auto-fluorescence and auto-luminescence, see supplementary methods.

In vivo experiments

458 Animals were housed in individually ventilated cages and received water and
459 standard food ad libitum. Female BALB/c mice (internal stock KU Leuven or Charles
460 River Laboratories) were infected at an age of 9-10 weeks. All animal experiments
461 were conducted in accordance with European directive 2010/63/EU and approved by
462 the animal ethics committee of KU Leuven (P006/2017, P103/2012).

463 *Preparation of Cryptococcus neoformans inoculum*

464 The bioluminescent C. *neoformans* strain was cultured in liquid Sabouraud medium
465 for 2-3 days at 30°C. As previously described (28), fungal cells were harvested by
466 centrifugation, washed twice with Dulbecco's PBS (Gibco, Paisley, UK), counted
467 using a Neubauer counting chamber and diluted to the desired concentration in PBS.
468 The number of CFUs in the inoculum was confirmed by plating on Sabouraud agar.

469 *Experiment 1: Systemic treatment in the meningoencephalitis model (Fig. 3A)*

470 Animals were anaesthetized using 1.5-2% isoflurane (IsoVET®, Primal Critical Care
471 Limited, West Drayton, UK) in 100% oxygen and infected by tail vein injection of
472 50,000 fungal cells in 100 µl of PBS to induce disseminated infection and subsequent
473 meningoencephalitis (28). Starting from day 3 p.i., animals (n = 4 per group) received
474 antifungal treatment by i.p. injection of L-AMB (10 mg/kg), saline, or FLC (75 mg/kg).
475 For the latter, we initially aimed to administer 150 mg/kg (corresponding to 800
476 mg/day in humans) based on previous reports of high-dose FLC treatment (47), but
477 we found that this was not feasible due to the limited solubility of FLC in saline. L-
478 AMB was dispersed in sterile water and diluted with 5% glucose solution prior to
479 injection, as per the manufacturer's instructions. 1 animal in the FLC group did not
480 develop infection, most likely due to inefficient i.v. injection and was excluded from
481 the analysis. BLI scans were performed on day 3 (prior to antifungal treatment), 4, 5,

6 and 7, while 2D and 3D MRI scans were done on day 4 and 6. BLI was performed prior to the daily dose of the antifungal, except on day 4.

Experiment 2: Systemic treatment in the cryptococcoma model (Fig. 3B)

Focal cryptococcal brain lesions were induced by intracranial stereotactic injection, based on a previously described rat model (48). Mice were anaesthetized by i.p. injection of ketamine (45-60 mg/kg, Nimatek®, Eurovet Animal Health, Bladel, The Netherlands) and medetomidine (0.6-0.8 mg/kg, Domitor®, Orion Pharma, Espoo, Finland). Fur on the head was clipped, the skin was disinfected and local analgesia was administered (2% lidocaine, Linisol®, Braun, Berlin, Germany). The animal's head was fixed in a stereotactic frame (Stoelting, Wood Dale, IL, USA) and 10,000 bioluminescent *Cryptococcus* cells were injected (1 µl, rate of 0.5 µl/min) in the striatum using a 10 µl Hamilton syringe with 30 gauge needle (Hamilton Company, Reno, NV, USA). Injection coordinates were 0.5 mm anterior and 2 mm lateral to bregma, and 3 mm from the dura. To prevent backflow of the injected cells, the burr hole was closed using dental filling resin (NanoFil® flowable light curing composite, AT&M Biomaterials, Beijing, China). The incision site was sutured and anesthesia was reversed by i.p. injection of atipamezole hydrochloride (0.5 mg/kg, Antisedan®, Orion Pharma). Additional animals were injected with a GFP-expressing *C. neoformans* H99 strain for histological analysis of the cryptococcoma model (see supplementary methods).

Starting from day 3 p.i., mice (n = 4 per group) received daily i.p. injections with saline, L-AMB (10 mg/kg) or FLC (75 mg/kg). A fourth group of animals received a single high dose of L-AMB (20 mg/kg) i.v., based on previous reports on the efficacy of this regimens (49). BLI and 2D MRI scans were performed on day 3 (prior to antifungal treatment), 6 and 9 p.i..

Experiment 3: Intracerebral treatment in the cryptococcoma model (Fig. 3C)

Focal cryptococcal brain lesions were induced by stereotactic injection. On day 6 and 8 p.i., mice (n = 5) received an intracranial stereotactic injection of L-AMB (2.5 µl of 0.6 mg/ml in sterile water) inside the brain lesion, at the same coordinates as used for induction. 2.5 µl was distributed in five steps of 0.5 µl, spaced every 0.5 mm between 4 and 2 mm from the dura. Control animals (n = 4) were injected with 2.5 µl of sterile water. Mice were scanned using BLI and MRI (2D) on day 6 (prior to the first treatment), 8 and 10.

Image acquisition and analysis

BLI

Mice were injected i.p. with D-luciferin solution (15 mg/ml) at a dose of 126 mg/kg prior to anesthesia (50). Immediately afterwards, animals were anaesthetized using 1.5-2% isoflurane in 100% oxygen. Ten to fifteen minutes after D-luciferin injection, mice were placed in prone position in an IVIS Spectrum imaging system (Perkin Elmer) equipped with Living Image Software (version 4.5.2). Consecutive images were acquired during 30 minutes using an exposure time of 1 minute, F/stop 1, subject height of 1.5 cm and medium binning. The total photon flux was quantified using Living Image Software (version 4.5.4). Regions of interest were located in the brain (cryptococcoma model: circular ROI of 1.8 cm diameter, meningoencephalitis model: rectangular ROI of 1.6 by 1.3 cm) or upper abdomen (including spleen and kidney region, 2.5 by 1.3 cm). Per animal and time point, the highest total photon flux obtained from all consecutive images was used for further statistical analysis.

Magnetic resonance imaging

MR scans were acquired using a 9.4T preclinical MRI scanner with 20 cm bore (Biospec 94/20) and a linearly polarized resonator (72 mm diameter) in combination with an actively decoupled mouse brain surface coil (all Bruker Biospin, Ettlingen, Germany). A physiological monitoring system (Small Animal Instruments Inc., Stony Brook, NY, US) was used to monitor the animals' breathing rate and body temperature during isoflurane anesthesia. After acquisition of localizer images, a 2D coronal T_2-weighted MR brain scan was acquired with the following parameters: spin-echo sequence, RARE factor of 8, TR/effective TE 4200/36.3 ms, field of view 2 x 1.5 cm, 12 slices with 0.5 mm slice thickness, 100 µm in plane resolution and a scan time of 1 min. A 2D axial brain scan was acquired with a RARE factor of 8, TR/effective TE 4200/36.3 ms, field of view 2 x 2 cm, 9 slices with 0.5 mm thickness and 0.2 mm slice gap, in plane resolution of 78.125 µm and a scan time of 1.66 min. Parameters for the 3D T_2-weighted brain MR scans (meningoencephalitis model) were: spin-echo sequence, RARE factor 10, TR/TE 1000/36 ms, FOV 2.4×1.5×0.83 cm, isotropic spatial resolution of approximately 94 µm and a scan time of 15 min.

Lesions were manually delineated on the 2D or 3D scans using the brush tool in ITK-SNAP (version 3.4.0, (51)). The reported lesion volume in the cryptococcoma model is the average volume obtained from the coronal and axial 2D scans. For the 3D scans in the meningoencephalitis model, the number of brain lesions and average volume per lesion was determined in ImageJ (version 1.49, National Institute of Health, USA, (52)) by using the 3D object counter (53) after applying a Watershed algorithm on the segmentation image.

CFU analysis

After the last imaging session, or when humane endpoints were reached, animals were sacrificed by i.p. injection of a pentobarbital overdose. The brains were isolated,

555 weighted and homogenized after addition of PBS. Serial 10-fold dilutions were plated
556 in triplicate on Sabouraud agar. After 3 days incubation at room temperature or 2
557 days at 30°C, the number of colonies was counted manually. All reported CFU
558 counts are expressed as CFUs/g weighted tissue. For correlations with the imaging
559 data, animals that succumbed to disease prior to the end of the experiments were
560 excluded.

561 **Statistical analysis**

562 Data were analyzed using Graphpad Prism (version 8.1.2). Time-kill curves were
563 analyzed using a two-way repeated measures ANOVA, followed by a Dunnett's post-
564 test to compare each treatment group to the control curve. *In vitro* data at specific
565 time points were analyzed using a one-way ANOVA with Dunnett's post-test
566 compared to the control setting.

567 Longitudinal *in vivo* imaging datasets were analyzed using a mixed-effects model
568 with Geisser-Greenhouse correction to investigate whether treatment effects were
569 significant. If no significant effect was found, only this p-value is reported. When
570 treatment was a significant factor, p-values for the comparison of specific treatment
571 groups to the control group (over all time points) are reported after using a Dunnett's
572 post-test. This was followed by a second Dunnett's post-test comparing the groups at
573 the specific time points (significance indicated on the graph). CFU data was analyzed
574 using an unpaired t-test or one-way ANOVA with Dunnett's post-test and linear
575 regression with Pearson correlation coefficients. *In vivo* BLI and CFU data were log-
576 transformed prior to statistical analysis.

Acknowledgements

The authors wish to thank Jens Wouters and Sarah Belderbos for their assistance and thank Dr. Kristof Govaerts for his guidance with the MRI quantification. We gratefully acknowledge Dr. Steffen Fieuws (L-BioStat, KU Leuven) for statistical advice. This work was funded by the European ERA-NET project 'CryptoView' (3rd call of the FP7 program Infect-ERA), the Research Foundation-Flanders (FWO, 1506114N) and KU Leuven (PF 10/017 (IMIR), CREA/14/015). L.V. is a PhD fellow strategic basic research at the FWO (151313). J.P. received a PhD grant for strategic basic research from the Agency for Innovation by Science and Technology (IWT, 141230). G.V.V. received a postdoctoral fellowship from the FWO (12N7615N).

Competing interests

Katrien Lagrou received consultancy fees from Pfizer, Abbott, MSD and SMB Laboratoires Brussels, she received travel support from Pfizer and MSD and speaker fees from Gilead, MSD, Roche, Abbott; all outside the submitted work.

References

1. Góralska K, Blaszkowska J, Dzikowiec M. 2018. Neuroinfections caused by fungi. Infection 46:443–459.
2. Schwartz S, Kontoyiannis DP, Harrison T, Ruhnke M. 2018. Advances in the diagnosis and treatment of fungal infections of the CNS. Lancet Neurol 17:362–372.
3. Enoch DA, Yang H, Aliyu SH, Micallef C. 2017. The Changing Epidemiology of Invasive Fungal Infections, p. 17–65. *In* . Humana Press, New York, NY.
4. Lee SC, Dickson DW, Casadevall A. 1996. Pathology of cryptococcal meningoencephalitis: Analysis of 27 patients with pathogenetic implications. Hum Pathol 27:839–847.
5. Williamson PR, Jarvis JN, Panackal AA, Fisher MC, Molloy SF, Loyse A, Harrison TS. Cryptococcal meningitis: epidemiology, immunology, diagnosis and therapy. Nat Rev Neurol 13:13–24.
6. Chen S, Sorrell T, Nimmo G, Speed B, Currie B, Ellis D, Marriott D, Pfeiffer T, Parr D, Byth K. 2000. Epidemiology and Host- and Variety-Dependent Characteristics of Infection Due to Cryptococcus neoformans in Australia and New Zealand. Clin Infect Dis 31:499–508.
7. Nguyen MH, Husain S, Clancy CJ, Peacock JE, Hung C-C, Kontoyiannis DP, Morris AJ, Heath CH, Wagener M, Yu VL. 2010. Outcomes of central nervous system cryptococcosis vary with host immune function: Results from a multi-center, prospective study. J Infect 61:419–426.
8. Roemer T, Krysan DJ. 2014. Antifungal drug development: challenges, unmet clinical needs, and new approaches. Cold Spring Harb Perspect Med 4:a019703.
9. Perfect JR. 2017. The antifungal pipeline: a reality check. Nat Rev Drug Discov 16:603–616.
10. Sloan D, Parris V. 2014. Cryptococcal meningitis: epidemiology and therapeutic options. Clin Epidemiol 6:169.
11. World Health Organization. 2018. Guidelines for the diagnosis, prevention and management of cryptococcal disease in HIV-infected adults, adolescents and children: supplement to the 2016 consolidated guidelines on the use of antiretroviral drugs for treating and preventing HIV infection.Who.
12. Sloan DJ, Dedicoat MJ, Lalloo DG. 2009. Treatment of cryptococcal meningitis in resource limited settings. Curr Opin Infect Dis 22:455–63.
13. Molloy SF, Kanyama C, Heyderman RS, Loyse A, Kouanfack C, Chanda D, Mfinanga S,

Temfack E, Lakhi S, Lesikari S, Chan AK, Stone N, Kalata N, Karunaharan N, Gaskell K, Peirse M, Ellis J, Chawinga C, Lontsi S, Ndong J-G, Bright P, Lupiya D, Chen T, Bradley J, Adams J, van der Horst C, van Oosterhout JJ, Sini V, Mapoure YN, Mwaba P, Bicanic T, Lalloo DG, Wang D, Hosseinipour MC, Lortholary O, Jaffar S, Harrison TS. 2018. Antifungal Combinations for Treatment of Cryptococcal Meningitis in Africa. N Engl J Med 378:1004–1017.

14. Krysan DJ. 2015. Toward improved anti-cryptococcal drugs: Novel molecules and repurposed drugs. Fungal Genet Biol 78:93–98.

15. Felton T, Troke PF, Hope WW. 2014. Tissue penetration of antifungal agents. Clin Microbiol Rev 27:68–88.

16. Capilla J, Clemons K V., Stevens DA. 2007. Animal models: an important tool in mycology. Med Mycol 45:657–684.

17. Hohl TM. 2014. Overview of vertebrate animal models of fungal infection. J Immunol Methods 410:100–12.

18. Avci P, Karimi M, Sadasivam M, Antunes-Melo WC, Carrasco E, Hamblin MR. 2018. *In-vivo* monitoring of infectious diseases in living animals using bioluminescence imaging. Virulence 9:28–63.

19. Vande Velde G, Kucharíková S, Van Dijck P, Himmelreich U. 2018. Bioluminescence imaging increases in vivo screening efficiency for antifungal activity against device-associated *Candida albicans* biofilms. Int J Antimicrob Agents 52:42–51.

20. Persyn A, Rogiers O, Brock M, Vande Velde G, Lamkanfi M, Jacobsen ID, Himmelreich U, Lagrou K, Van Dijck P, Kucharíková S. 2019. Monitoring of Fluconazole and Caspofungin Activity against In Vivo Candida glabrata Biofilms by Bioluminescence Imaging. Antimicrob Agents Chemother 63.

21. Vande Velde G, Kucharíková S, Schrevens S, Himmelreich U, Van Dijck P. 2014. Towards non-invasive monitoring of pathogen-host interactions during Candida albicans biofilm formation using in vivo bioluminescence. Cell Microbiol 16:115–30.

22. Brock M, Jouvion G, Droin-Bergère S, Dussurget O, Nicola M-A, Ibrahim-Granet O. 2008. Bioluminescent *Aspergillus fumigatus*, a new tool for drug efficiency testing and in vivo monitoring of invasive aspergillosis. Appl Environ Microbiol 74:7023–35.

23. Galiger C, Brock M, Jouvion G, Savers A, Parlato M, Ibrahim-Granet O. 2013. Assessment of efficacy of antifungals against *Aspergillus fumigatus*: value of real-time bioluminescence imaging. Antimicrob Agents Chemother 57:3046–59.

24. Kaskova ZM, Tsarkova AS, Yampolsky I V. 2016. 1001 lights: Luciferins, luciferases, their mechanisms of action and applications in chemical analysis, biology and medicine. Chem Soc Rev. Royal Society of Chemistry.

25. Binder U, Navarro-Mendoza MI, Naschberger V, Bauer I, Nicolas FE, Pallua JD, Lass-Flörl C, Garre V, Binder U, Navarro-Mendoza MI, Naschberger V, Bauer I, Nicolas FE, Pallua JD, Lass-Flörl C, Garre V. 2018. Generation of A *Mucor circinelloides* Reporter Strain—A Promising New Tool to Study Antifungal Drug Efficacy and Mucormycosis. Genes (Basel) 9:613.

26. Poelmans J, Himmelreich U, Vanherp L, Zhai L, Hillen A, Holvoet B, Belderbos S, Brock M, Maertens J, Vande Velde G, Lagrou K. 2018. A Multimodal Imaging Approach Enables *In Vivo* Assessment of Antifungal Treatment in a Mouse Model of Invasive Pulmonary Aspergillosis. Antimicrob Agents Chemother 62:AAC.00240-18.

27. Jacobsen ID, Lüttich A, Kurzai O, Hube B, Brock M. 2014. In vivo imaging of disseminated murine *Candida albicans* infection reveals unexpected host sites of fungal persistence during antifungal therapy. J Antimicrob Chemother 69:2785–2796.

28. Vanherp L, Ristani A, Poelmans J, Hillen A, Lagrou K, Janbon G, Brock M, Himmelreich U, Vande Velde G. 2019. Sensitive bioluminescence imaging of fungal dissemination to the brain in mouse models of cryptococcosis. Dis Model Mech 12:dmm039123.

29. Dorsaz S, Coste AT, Sanglard D. 2017. Red-Shifted Firefly Luciferase Optimized for *Candida albicans In vivo* Bioluminescence Imaging. Front Microbiol 8:1478.

30. Palacios DS, Dailey I, Siebert DM, Wilcock BC, Burke MD. 2011. Synthesis-enabled functional group deletions reveal key underpinnings of amphotericin B ion channel and antifungal activities. Proc Natl Acad Sci 108:6733–6738.

31. Bolard J. 1986. How do the polyene macrolide antibiotics affect the cellular membrane properties? Biochim Biophys Acta 864:257–304.

32. Virta M, Åkerman KEO, Saviranta P, Oker-Blom C, Karp MT. 1995. Real-time measurement of cell permeabilization with low-molecular-weight membranolytic agents. J Antimicrob Chemother 36:303–315.

681 33. te Welscher YM, ten Napel HH, Balagué MM, Souza CM, Riezman H, de Kruijff B, Breukink E.
682 2008. Natamycin blocks fungal growth by binding specifically to ergosterol without
683 permeabilizing the membrane. J Biol Chem 283:6393–401.
684 34. Van Dijck P, Sjollema J, Cammue BP, Lagrou K, Berman J, d'Enfert C, Andes DR, Arendrup
685 MC, Brakhage AA, Calderone R, Cantón E, Coenye T, Cos P, Cowen LE, Edgerton M, Espinel-
686 Ingroff A, Filler SG, Ghannoum M, Gow NAR, Haas H, Jabra-Rizk MA, Johnson EM, Lockhart
687 SR, Lopez-Ribot JL, Maertens J, Munro CA, Nett JE, Nobile CJ, Pfaller MA, Ramage G,
688 Sanglard D, Sanguinetti M, Spriet I, Verweij PE, Warris A, Wauters J, Yeaman MR, Zaat SAJ,
689 Thevissen K. 2018. Methodologies for in vitro and in vivo evaluation of efficacy of antifungal
690 and antibiofilm agents and surface coatings against fungal biofilms. Microb cell (Graz, Austria)
691 5:300–326.
692 35. Ayzenberg I, Schlevogt S, Metzdorf J, Stahlke S, Pedreitturia X, Hunfeld A, Couillard-Despres
693 S, Kleiter I. 2015. Analysis of Neurogenesis during Experimental Autoimmune
694 Encephalomyelitis Reveals Pitfalls of Bioluminescence Imaging. PLoS One 10:e0118550.
695 36. Hospenthal DR, Bennett JE. 2000. Persistence of Cryptococcomas on Neuroimaging. Clin
696 Infect Dis 31:1303–1306.
697 37. Perfect JR, Dismukes WE, Dromer F, Goldman DL, Graybill JR, Hamill RJ, Harrison TS,
698 Larsen RA, Lortholary O, Nguyen M-H, Pappas PG, Powderly WG, Singh N, Sobel JD, Sorrell
699 TC. 2010. Clinical practice guidelines for the management of cryptococcal disease: 2010
700 update by the infectious diseases society of america. Clin Infect Dis 50:291–322.
701 38. Ulett KB, Cockburn JWJ, Jeffree R, Woods ML. 2017. Cerebral cryptococcoma mimicking
702 glioblastoma. BMJ Case Rep 2017.
703 39. Pai MP, Sakoglu U, Peterson SL, Lyons CR, Sood R. 2009. Characterization of BBB
704 permeability in a preclinical model of cryptococcal meningoencephalitis using magnetic
705 resonance imaging. J Cereb Blood Flow Metab 29:545–53.
706 40. Takemoto K, Yamamoto Y, Ueda Y. 2006. Influence of the Progression of Cryptococcal
707 Meningitis on Brain Penetration and Efficacy of AmBisome in a Murine Model. Chemotherapy
708 52:271–278.
709 41. Lu R, Hollingsworth C, Qiu J, Wang A, Hughes E, Xin X, Konrath KM, Elsegeiny W, Park Y-D,
710 Atakulu L, Craft JC, Tramont EC, Mannino R, Williamson PR. 2019. Efficacy of Oral

711 Encochleated Amphotericin B in a Mouse Model of Cryptococcal Meningoencephalitis. MBio
712 10:e00724-19.
713 42. Pasquier E, Kunda J, De Beaudrap P, Loyse A, Temfack E, Molloy SF, Harrison TS, Lortholary
714 O. 2018. Long term mortality and disability in Cryptococcal Meningitis: a systematic literature
715 review. Clin Infect Dis 66:1122–1132.
716 43. Aye C, Henderson A, Yu H, Norton R. 2016. Cryptococcosis: the impact of delay to diagnosis.
717 Clin Microbiol Infect 22:632–635.
718 44. Bellmann R, Smuszkiewicz P. 2017. Pharmacokinetics of antifungal drugs: practical
719 implications for optimized treatment of patients. Infection 45:737.
720 45. Vogelsinger H, Weiler S, Djanani A, Kountchev J, Bellmann-Weiler R, Wiedermann CJ,
721 Bellmann R. 2006. Amphotericin B tissue distribution in autopsy material after treatment with
722 liposomal amphotericin B and amphotericin B colloidal dispersion. J Antimicrob Chemother
723 57:1153–1160.
724 46. Voelz K, Johnston SA, Rutherford JC, May RC. 2010. Automated analysis of cryptococcal
725 macrophage parasitism using GFP-tagged cryptococci. PLoS One 5:e15968.
726 47. Santos JRA, Ribeiro NQ, Bastos RW, Holanda RA, Silva LC, Queiroz ER, Santos DA. 2017.
727 High-dose fluconazole in combination with amphotericin B is more efficient than monotherapy
728 in murine model of cryptococcosis. Sci Rep 7:4661.
729 48. Himmelreich U, Dzendrowskyj TE, Allen C, Dowd S, Malik R, Shehan BP, Russell P, Mountford
730 CE, Sorrell TC. 2001. Cryptococcomas distinguished from gliomas with MR spectroscopy: an
731 experimental rat and cell culture study. Radiology 220:122–8.
732 49. Lestner J, McEntee L, Johnson A, Livermore J, Whalley S, Schwartz J, Perfect JR, Harrison T,
733 Hope W. 2017. Experimental Models of Short Courses of Liposomal Amphotericin B for
734 Induction Therapy for Cryptococcal Meningitis. Antimicrob Agents Chemother 61:e00090-17.
735 50. Aswendt M, Adamczak J, Couillard-Despres S, Hoehn M, Bailly C, Gaensler K. 2013. Boosting
736 Bioluminescence Neuroimaging: An Optimized Protocol for Brain Studies. PLoS One 8:e55662.
737 51. Yushkevich PA, Piven J, Hazlett HC, Smith RG, Ho S, Gee JC, Gerig G. 2006. User-guided 3D
738 active contour segmentation of anatomical structures: Significantly improved efficiency and
739 reliability. Neuroimage 31:1116–1128.
740 52. Schneider CA, Rasband WS, Eliceiri KW. 2012. NIH Image to ImageJ: 25 years of image

741 analysis. Nat Methods 9:671–675.

742 53. Bolte S, Cordelières FP. 2006. A guided tour into subcellular colocalization analysis in light

743 microscopy. J Microsc 224:213–232.

Figure legends

Figure 1: *In vitro* bioluminescence assay of antifungal effects. Amphotericin B deoxycholate (AMB-d, 0.1 mg/ml), fluconazole (FLC, 0.5 mg/ml), or sterile water (control) were added to pre-grown (24 h old) liquid cultures. Bioluminescence was measured immediately after, 2, 4, 6, 8, 24, 48 and 72 hours after antifungal addition by adding D-luciferin (0.15 µg/ml) to samples of the culture. The bioluminescence signal is expressed relative to the signal obtained immediately after addition of antifungal (0 h). Curves were significantly different for AMB-d ($p<0.0001$) and fluconazole ($p=0.0152$) compared to the control curve. Two-way repeated measures ANOVA with Dunnett's multiple comparison post-test. Graph shows mean ± SD.

Figure 2: Temporal profile of the bioluminescence signals in response to different antifungal compounds. Bioluminescent *C. neoformans* cells in liquid culture (20 h old) were exposed to various doses of antifungals and the bioluminescence was measured in real time at the indicated time points by adding D-luciferin to culture samples. A) Amphotericin B deoxycholate (AMB-d) showed a dose-dependent antifungal effect. Bioluminescence increased transiently shortly after addition. B) Liposomal amphotericin B (L-AMB) induced a similar but more delayed response. C) Fluconazole showed a modest antifungal effect at the tested concentrations. D) Exposure to natamycin induced a dose-dependent killing of the fungi. A transient increase was only observed for the highest concentration tested. E) Sodium dodecyl sulphate (SDS) caused a rapid dose-dependent decrease in bioluminescence. Graphs show mean ± SD.

Figure 3: Experimental set-ups for *in vivo* imaging *of* treatment efficacy in delayed-treatment models. A) Systemic treatment in the model of meningoencephalitis following disseminated disease. B) Systemic treatment in the cryptococcoma model. C) Intracerebral treatment in the cryptococcoma model. Abbreviations: i.cr.: intracranial; i.p.: intraperitoneal; i.v.: intravenous; BL: baseline scans to assess infection status prior to initiation of treatment.

Figure 4: BLI of antifungal treatment efficacy in a model of cryptococcal meningoencephalitis. Animals (n = 4 per group) were intravenously injected with 50,000 bioluminescent *C. neoformans* cells and received daily injections with saline, liposomal amphotericin B (L-AMB, 10 mg/kg) or fluconazole (FLC, 75 mg/kg) starting from day 3 p.i.. One animal in the FLC group did not have an established infection and was excluded from further analysis (indicated with * on the images and with grey dashed line on the graphs). A) BLI for the individual animals. B) Quantification of the total photon flux in the brain region. The curves of FLC treated animals were significantly different from the saline group (p=0.016), but not for L-AMB treated animals (p=0.7376). On day 4, animals were injected with L-AMB shortly before BLI acquisition, leading to a significantly increased bioluminescence. C) The total photon flux in the abdominal region was significantly lower in the L-AMB group compared to the saline group (p=0.0001), but not for the FLC group (p=0.4374). Graphs show individual data points, mixed-effects model statistics with Dunnett's post-test. (-) indicates that animals were lost to follow-up.

Figure 5: Brain MRI after antifungal treatment in the meningoencephalitis model. Daily antifungal treatment with liposomal amphotericin B (L-AMB, 10 mg/kg), fluconazole (FLC, 75 mg/kg) or saline (n = 4 each) was initiated 3 days after intravenous injection with 50,000 *C. neoformans* cells. A) Slice of the 2D coronal MR images for the individual animals (1 slice / animal). B) The total lesion volume quantified from 3D MR images showed a significant effect for FLC-treatment (p=0.0066) but not for L-AMB (p=0.2095). C). Treatment did not have a significant effect (p=0.8561) on the number of lesions. D) The average lesion volume was significantly lower in the FLC-treated animals (p=0.0007), but not in animals receiving L-AMB treatment (p=0.9740). Graphs show individual data points, mixed-effects model statistics with Dunnett's post-test. (-) indicates animals lost to follow-up, * indicates one animal with unsuccessful induction of infection.

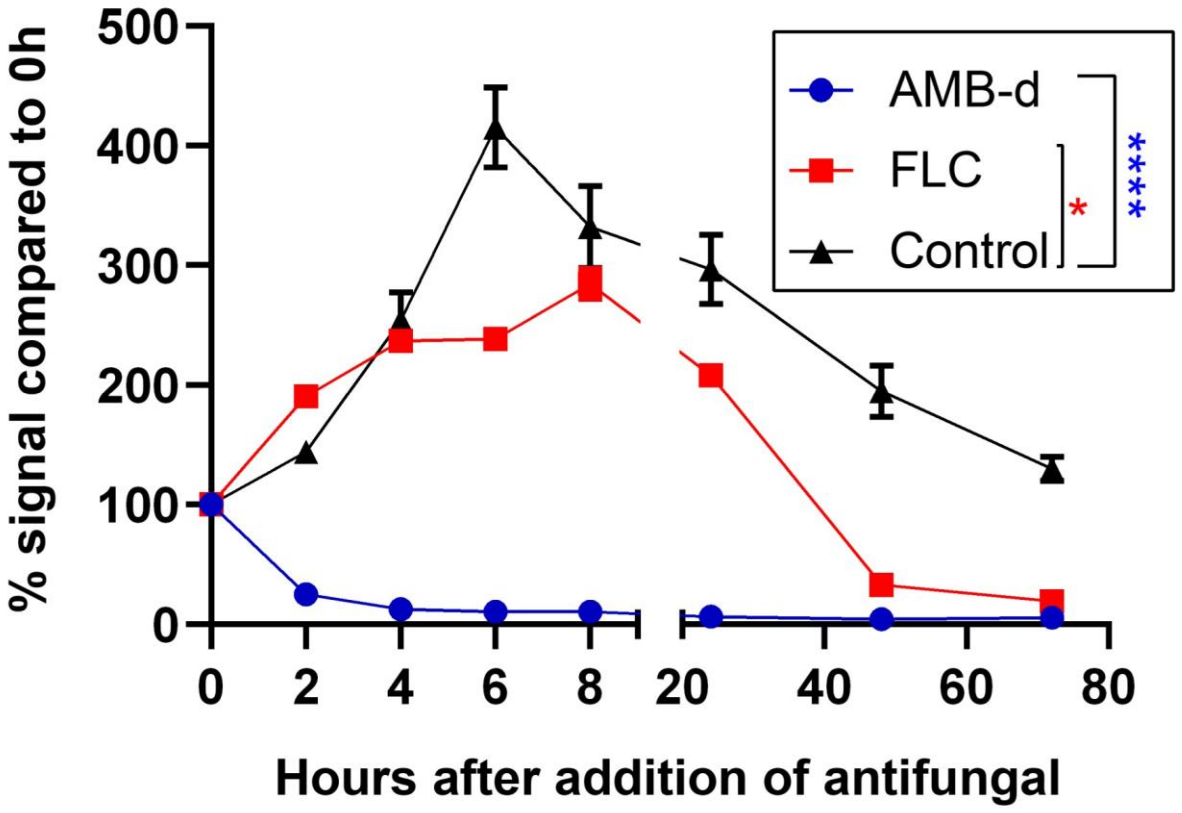
Figure 6: CFU analysis of the brain, spleen and kidneys after antifungal treatment in the meningoencephalitis model. Disseminated infection was induced by intravenous injection of 50,000 *C. neoformans* cells. Fungal load analysis was performed after the last imaging session or when animals were sacrificed for humane endpoints. A) Liposomal amphotericin B (L-AMB) and fluconazole (FLC) treatment induced a small reduction in the fungal load in the brain (p=0.0103 and p=0.0054, respectively). B) FLC treatment reduced the fungal load in the spleen (p=0.0128), while for L-AMB no fungal cells could be recovered (p<0.0001). C) L-AMB and FLC treatment lowered the fungal load in the kidneys (p<0.0001 and p=0.0023, respectively). Graphs show mean ± SD, one-way ANOVA with Dunnett's post-test.

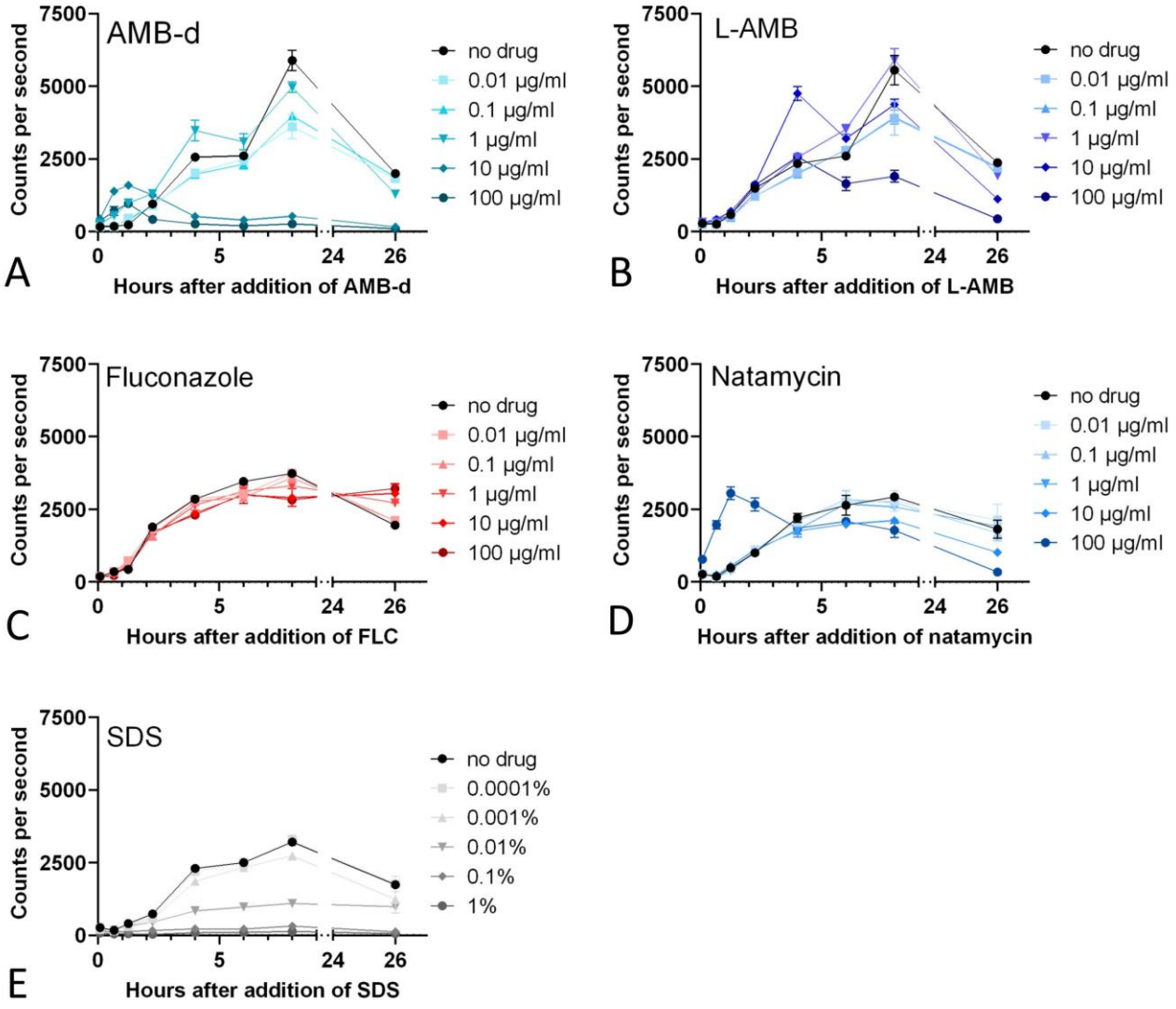
Figure 7: BLI and MRI of antifungal treatment efficacy following systemic treatment in the cryptococcoma model. Focal cryptococcomas were induced by stereotactic injection of 10,000 bioluminescent *C. neoformans* cells. Treatment (n=4 per group) was initiated on day 3 by daily i.p. injection of fluconazole (FLC, 75 mg/kg) or liposomal amphotericin B (L-AMB, 10 mg/kg), or a single i.v. dose (20 mg/kg) of L-AMB was given on day 3. A) BLI of treated animals. B) Coronal MRI slices for the corresponding animals (1 slice per animal). C) Quantification of the BLI signal in the brain region. Statistics did not show an overall significant effect of treatment (p=0.2977). D) Lesion volume quantified from the MR images showed an overall significant effect of treatment (p=0.0354), but no significant differences between the saline and treatment groups. Animals with higher bioluminescence and MRI-based evidence of cryptococcomas invading the ventricle are indicated with (*) on the images and open symbols on the graphs. Graphs show individual data points, mixed-effect model statistics with Dunnett's post-test. (-) indicates that animals were lost to follow-up.

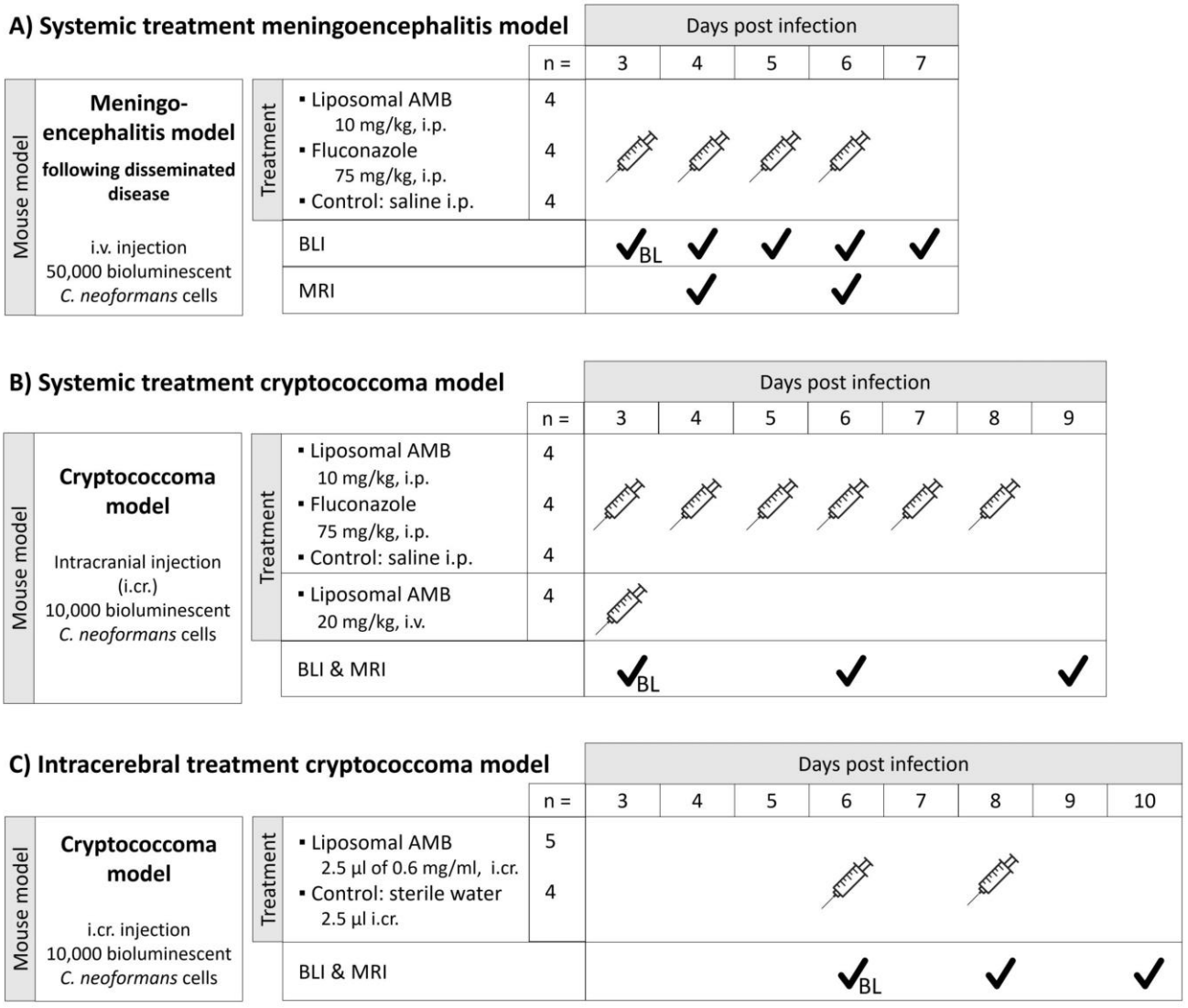
Figure 8: CFU analysis of the brains after systemic treatment in the cryptococcoma model and correlation with imaging readouts. A) Treatment induced a small but not significant decrease in the fungal brain load in animals treated daily with fluconazole (FLC) or liposomal amphotericin B (L-AMB). No significant differences were found (overall p-value = 0.0816). The animal with the notably higher brain fungal load in the L-AMB groups displayed spreading of the infection towards the forebrain. B-C) Quantification of *in vivo* BLI (B) and lesion volume obtained from MRI (C) correlated well with the fungal burden in the brain. When animals with spreading of the cryptococcomas to the ventricles (open symbols, see Fig. 7) were excluded, the correlation of BLI and CFU results was strengthened (r= 0.7491, p=0.0050). Graphs show data from individual animals. One-way ANOVA with Dunnett's post-test or Pearson correlation coefficients with linear regression and 95% confidence bands.

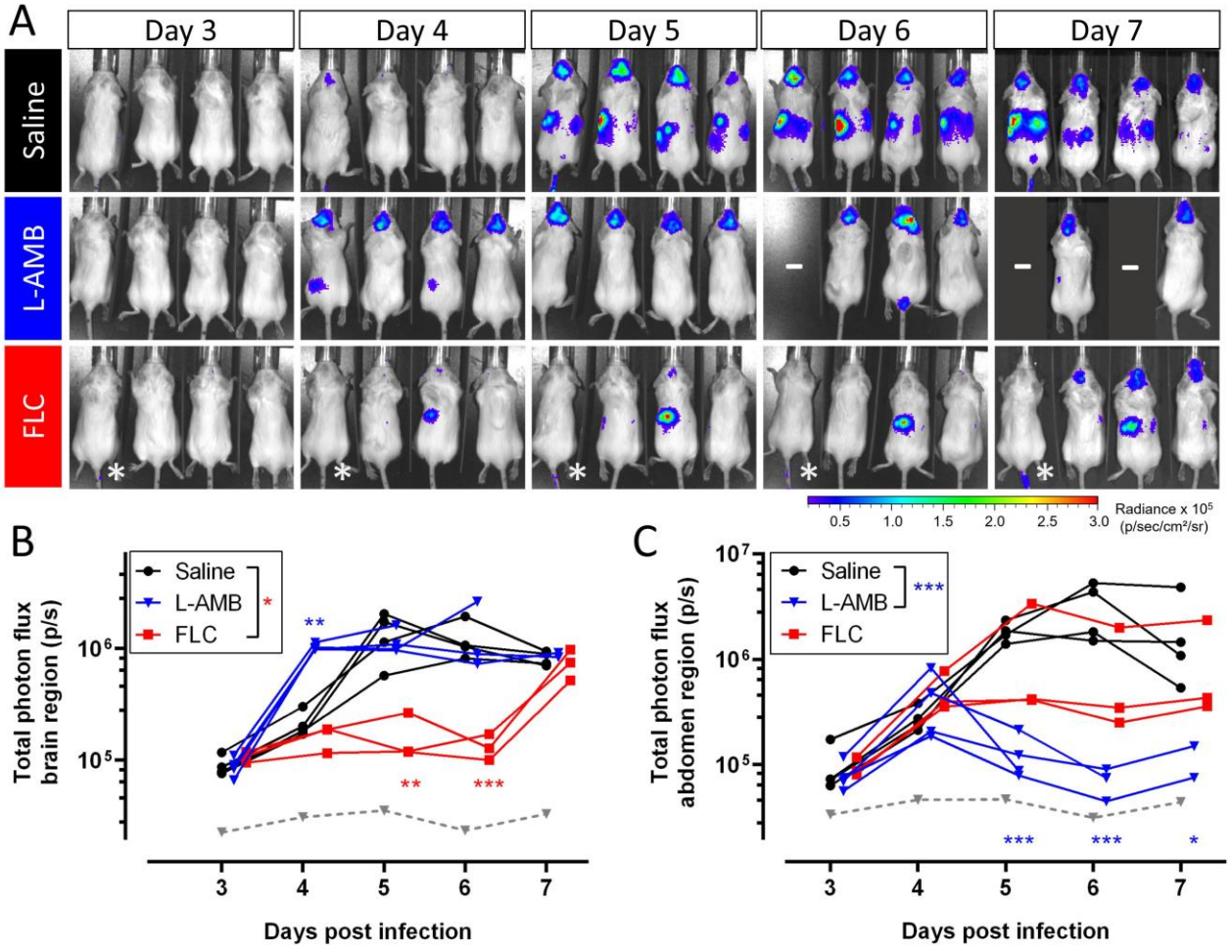
Figure 9: BLI and MRI of intracerebral treatment of cryptococcomas. Animals were stereotactically injected with 10,000 *C. neoformans* cells and liposomal amphotericin B (L-AMB) (n = 5) or sterile water (n = 4) was injected inside the brain lesion on day 6 and 8 p.i.. A) BLI of the infected animals on day 6 (before treatment), 8 and 10 p.i. B) Slice of the coronal 2D brain MRI for the same animals, showing a small hyperintense region in the lesion at the site of injection (red arrows). C) Quantification of the bioluminescence from the brain. D) Quantification of the lesion volume on MRI. No significant effect of the treatment was found for the BLI or MRI results at group level (p=0.2725 and p=0.4396, respectively). Numbers on the graphs correspond to the specific animals on the images. Graphs show individual data

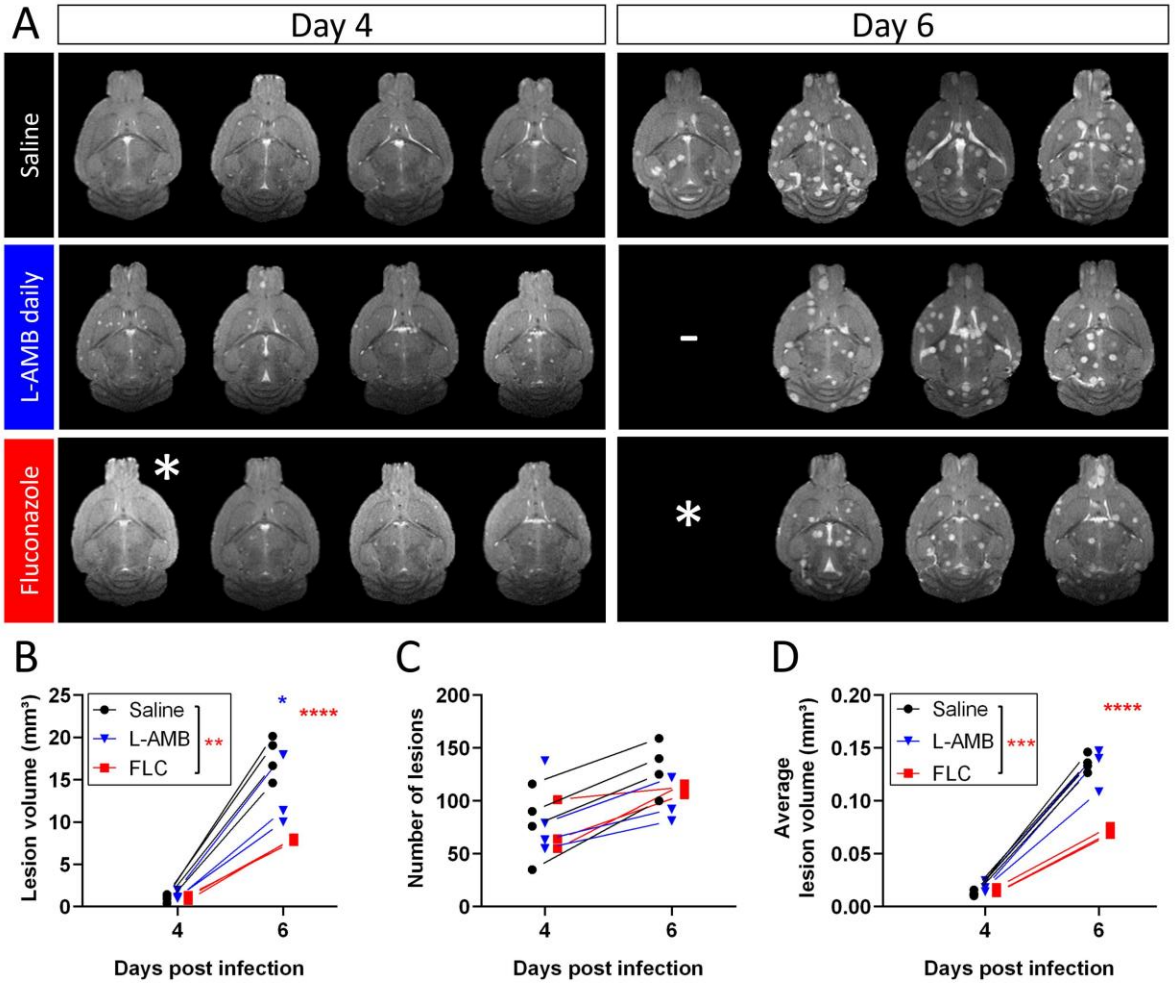
846 points, mixed-effect model statistics with Dunnett's post-test. (-) indicates that
847 animals were lost to follow-up.

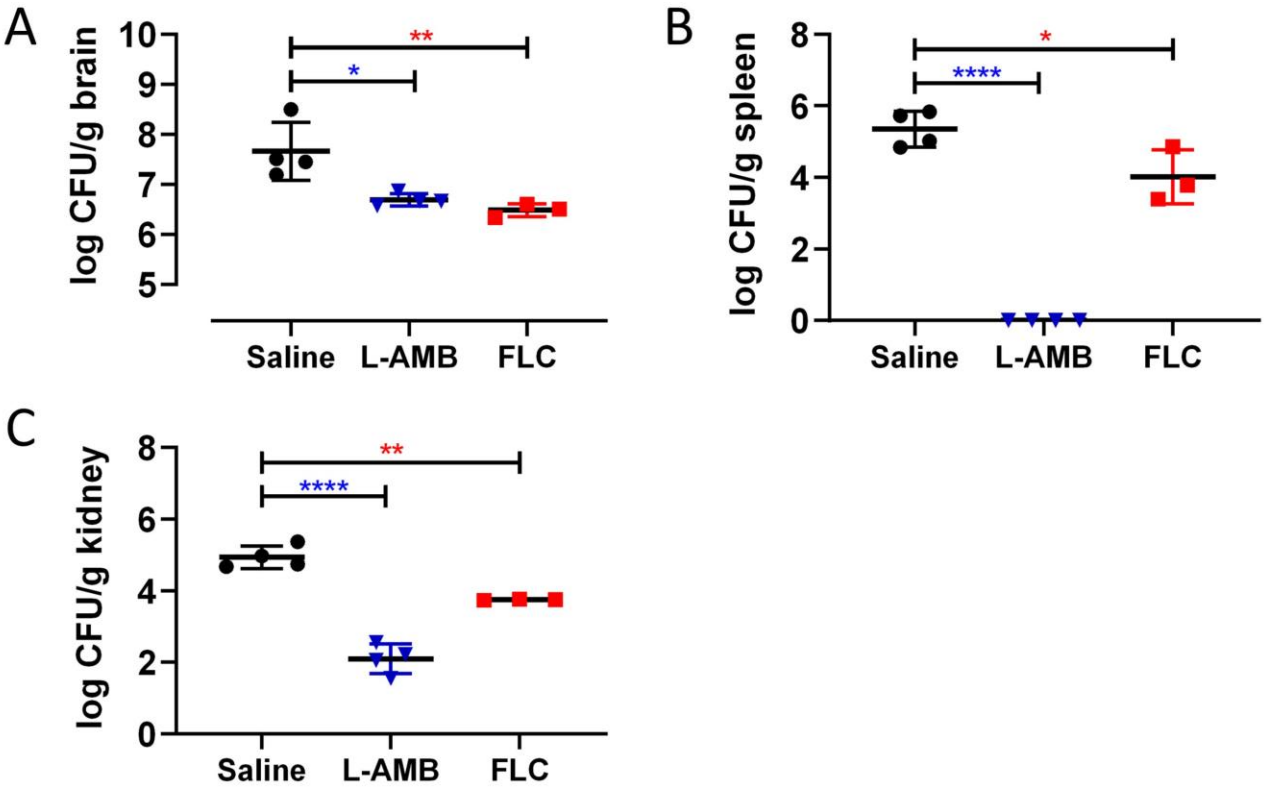

% signal compared to 0h
500
400
300
200
100
0
0
2
4
6
8
20
40
60
80
Hours after addition of antifungal
AMB-d
FLC
Control
*
*****

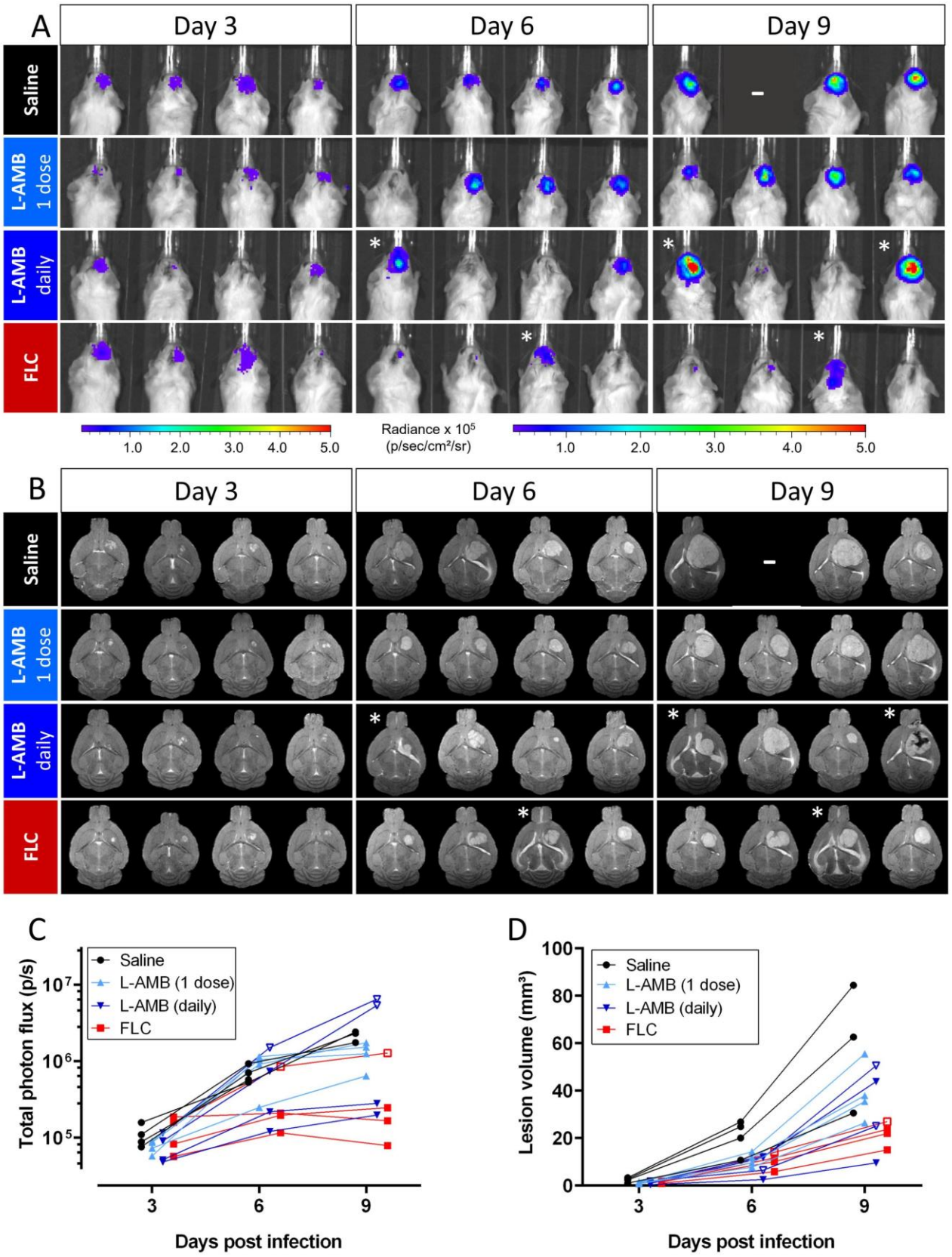

AMB-d
Counts per second
7500
5000
2500
0
0
5
24
26
Hours after addition of AMB-d
no drug
0.01 µg/ml
0.1 µg/ml
1 µg/ml
10 µg/ml
100 µg/ml
A
L-AMB
Hours after addition of L-AMB
B
Fluconazole
Hours after addition of FLC
C
Natamycin
Hours after addition of natamycin
D
SDS
no drug
0.0001%
0.001%
0.01%
0.1%
1%
Hours after addition of SDS
E

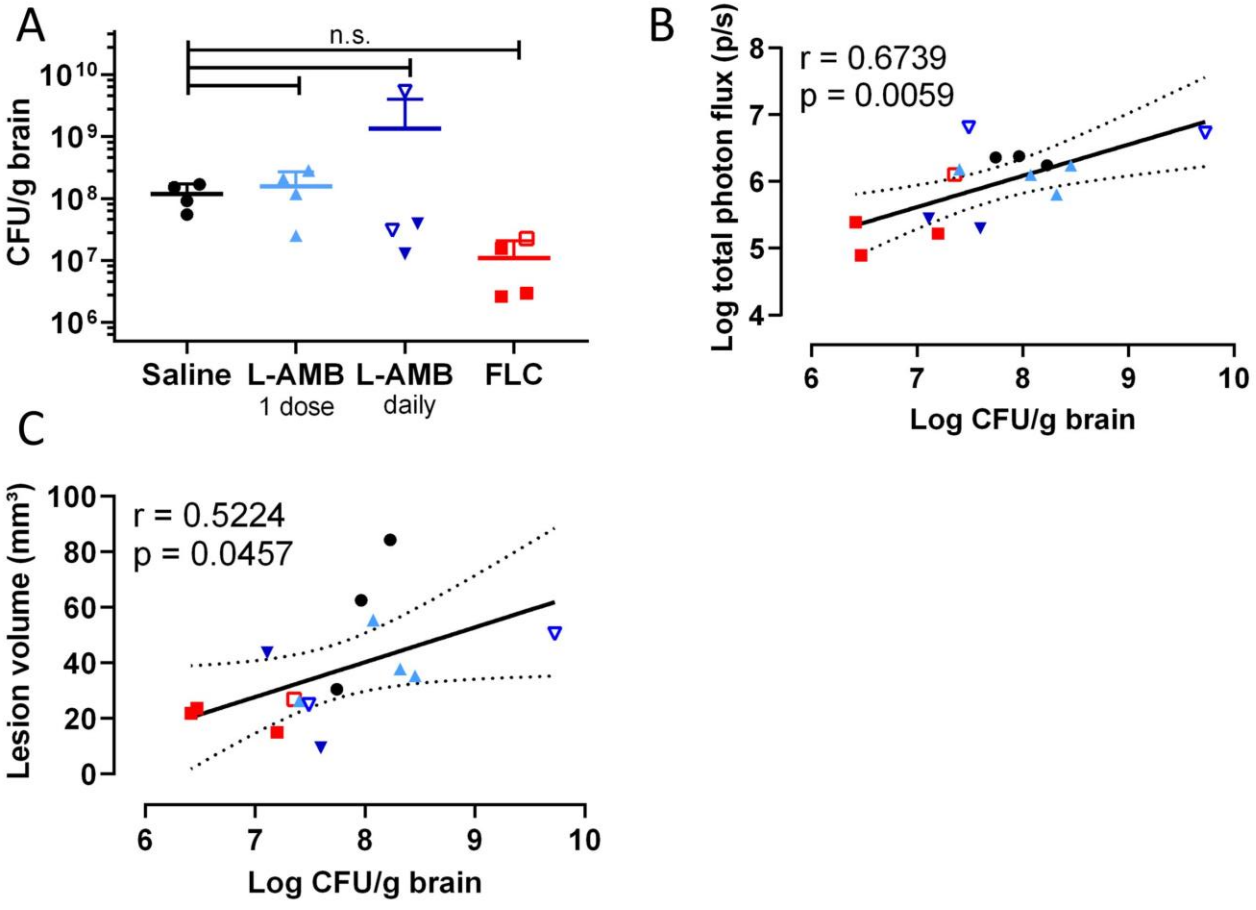

A) Systemic treatment meningoencephalitis model
Days post infection
n =
3
4
5
6
7
Mouse model
Meningo-encephalitis model
following disseminated disease
i.v. injection
50,000 bioluminescent
C. neoformans cells
Treatment
▪ Liposomal AMB
10 mg/kg, i.p.
4
▪ Fluconazole
75 mg/kg, i.p.
4
▪ Control: saline i.p.
4
BLI
BL
MRI
B) Systemic treatment cryptococcoma model
Days post infection
n =
3
4
5
6
7
8
9
Mouse model
Cryptococcoma model
Intracranial injection
(i.cr.)
10,000 bioluminescent
C. neoformans cells
Treatment
▪ Liposomal AMB
10 mg/kg, i.p.
4
▪ Fluconazole
75 mg/kg, i.p.
4
▪ Control: saline i.p.
4
▪ Liposomal AMB
20 mg/kg, i.v.
4
BLI & MRI
BL
C) Intracerebral treatment cryptococcoma model
Days post infection
n =
3
4
5
6
7
8
9
10
Mouse model
Cryptococcoma model
i.cr. injection
10,000 bioluminescent
C. neoformans cells
Treatment
▪ Liposomal AMB
2.5 µl of 0.6 mg/ml, i.cr.
5
▪ Control: sterile water
2.5 µl i.cr.
4
BLI & MRI
BL

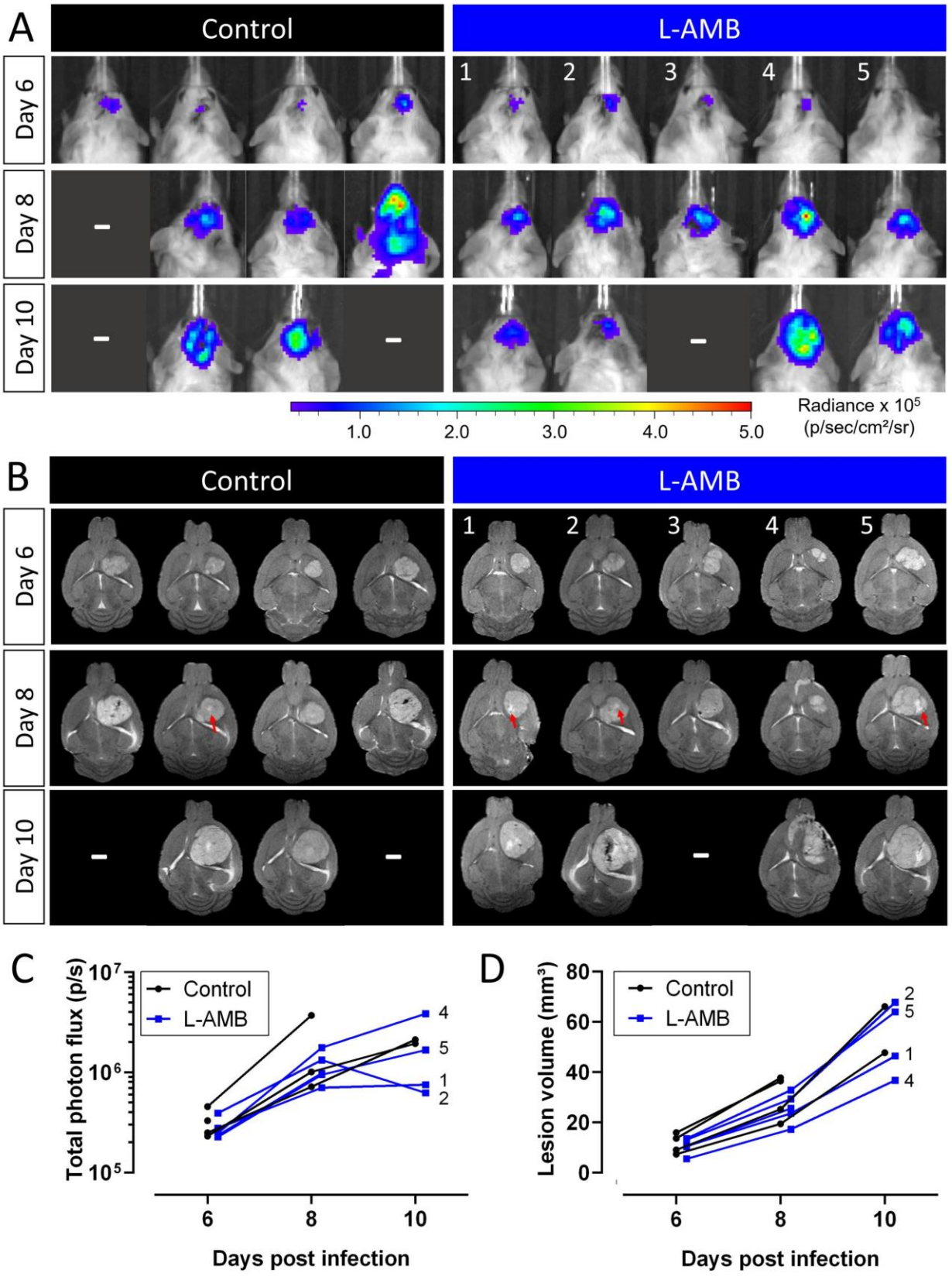

A
Day 3
Day 4
Day 5
Day 6
Day 7
Saline
L-AMB
FLC
0.5
1.0
1.5
2.0
2.5
3.0
Radiance x 10^5 (p/sec/cm²/sr)
B
Total photon flux brain region (p/s)
Saline
L-AMB
FLC
Days post infection
C
Total photon flux abdomen region (p/s)
Saline
L-AMB
FLC
Days post infection


A
Day 4
Day 6
Saline
L-AMB daily
Fluconazole
*
-
*
B
Lesion volume (mm³)
25
20
15
10
5
0
Saline
L-AMB
FLC
**
*
****
4
6
Days post infection
C
Number of lesions
200
150
100
50
0
4
6
Days post infection
D
Average lesion volume (mm³)
0.20
0.15
0.10
0.05
0.00
Saline
L-AMB
FLC
***
****
4
6
Days post infection


A
log CFU/g brain
10
9
8
7
6
5
**
*
Saline
L-AMB
FLC
B
log CFU/g spleen
8
6
4
2
0
*
****
Saline
L-AMB
FLC
C
log CFU/g kidney
8
6
4
2
0
**
****
Saline
L-AMB
FLC


A
Day 3
Day 6
Day 9
Saline
L-AMB 1 dose
L-AMB daily
FLC
1.0 2.0 3.0 4.0 5.0
Radiance x 10^5 (p/sec/cm²/sr)
1.0 2.0 3.0 4.0 5.0
B
Day 3
Day 6
Day 9
Saline
L-AMB 1 dose
L-AMB daily
FLC
C
Total photon flux (p/s)
10^7
10^6
10^5
Saline
L-AMB (1 dose)
L-AMB (daily)
FLC
3
6
9
Days post infection
D
Lesion volume (mm³)
100
80
60
40
20
0
Saline
L-AMB (1 dose)
L-AMB (daily)
FLC
3
6
9
Days post infection


A
n.s.
CFU/g brain
10^{10}
10^{9}
10^{8}
10^{7}
10^{6}
Saline
L-AMB
1 dose
L-AMB
daily
FLC
B
Log total photon flux (p/s)
r = 0.6739
p = 0.0059
Log CFU/g brain
C
Lesion volume (mm^3)
r = 0.5224
p = 0.0457
Log CFU/g brain


A
Control
L-AMB
Day 6
Day 8
Day 10
1
2
3
4
5
1.0
2.0
3.0
4.0
5.0
Radiance x 10⁵
(p/sec/cm²/sr)
B
Control
L-AMB
Day 6
Day 8
Day 10
1
2
3
4
5
C
Total photon flux (p/s)
10⁷
10⁶
10⁵
Control
L-AMB
4
5
1
2
6
8
10
Days post infection
D
Lesion volume (mm³)
80
60
40
20
0
Control
L-AMB
2
5
1
4
6
8
10
Days post infection